Article

Nonthermal Plasma Induced Fabrication of Solid Acid Catalysts for Glycerol Dehydration to Acrolein

Lu Liu and Xiaofei Philip Ye *

Department of Biosystems Engineering and Soil Science, The University of Tennessee, Knoxville, TN 37996, USA; LuLiuconsulting@outlook.com

* Correspondence: xye2@utk.edu; Tel.: +1-(865)-974-7129; Fax: +1-(865)-974-4514

Abstract: The feasibility of fabricating better solid acid catalysts using nonthermal plasma (NTP) technology for biobased acrolein production is demonstrated. NTP discharge exposure was integrated in catalyst fabrication in air or argon atmosphere. The fabricated catalysts were characterized by Brunauer–Emmett–Teller surface area analysis, temperature-programmed desorption of ammonia, X-ray powder diffraction and Fourier-transform infrared spectroscopy of pyridine adsorption, in comparison to regularly prepared catalysts as a control. Further, kinetic results collected via glycerol dehydration experiments were compared, and improvement in acrolein selectivity was displayed when the catalyst was fabricated in the argon NTP, but not in the air NTP. Possible mechanisms for the improvement were also discussed.

Keywords: catalyst fabrication; nonthermal plasma; glycerol; acrolein; Brønsted acid site; Lewis acid site

1. Introduction

The application of nonthermal plasma (NTP) for the surface modification of materials to render desirable properties have been well documented, such as the improvement of adhesion strength of coating, the generation of ultrafine particles, the deposition of catalytically active species, and the reduction of metal-catalysts, etc. [1,2]. NTP has also been used in fabricating supported metal catalysts to improve selectivity and efficiency in some chemical processes [3]. Halverson and Cocke [4] prepared Ru/Al_2O_3 with highly dispersed metallic particles by impregnation on NTP-grown alumina in an oxygen and water vapor environment. Alumina supported $LaMO_x$ (M denotes one of Co, Mn, or Ni) films were developed by radio-frequency NTP spray deposition, and different catalytic activities were reported as compared to the regularly prepared ones [5]. Vissokov [6] found that NTP could help produce ultradispersed catalysts due to changes in the nanostructural and physicochemical properties; as a result, 15–20% higher activity was achieved. Usually, better dispersion of the active compound on a catalyst support leads to better catalysts [1].

NTP treatment has been reported as a substitute for thermal calcination process of catalysts; significant reduction in treatment temperature and time and chemical activation were some of the major advantages of this novel approach [7]. Microwave NTP could introduce a certain level of local heating compared to other NTP techniques. Sugiyama et al. [7] used microwave NTP treatment to anneal a catalyst, and this catalyst improved the selectivity to the desired product, as compared to conventional calcination. This NTP annealing process also showed the advantage of reducing treatment time, providing similar or better reduction of metal oxide as compared to hours of conventional calcination [8]. Zhang et al. [9] found that using NTP glow discharge could activate Ni/α-Al_2O_3 and greatly improve its activity and stability in the syngas production from methane. A zeolite template could be removed when it was treated with a radio-frequency NTP [10]. Usually high-temperature calcination would cause the separation of a metal phase [11], the agglomeration into large metal particles [12,13], or the framework destruction, which

would negatively affect catalytic activities [1]. NTP treatment has been found as a solution to these problems, with additional beneficial modification to the catalyst surface. Guo et al. [14] found that the exposure to NTP discharge enhanced the specific surface area of manganese oxide/alumina/nickel foam; the granularity of the catalyst surface became smaller, and the distribution was more uniform after NTP exposure. Studies of treated resins have revealed that NTP discharge could be the cause of the changes in the surface oxygen content, surface morphologies, and surface energy [15]. A claim was made in Veprek's review on NTP [16] that the radiation damage caused by ion implantation increased the internal surface area of the catalysts, because the ion implantation with high energy was able to modify a layer of nitrided steel up to several micrometers deep. Yagodovskaya et al. [11] used NTP glow discharge to avoid the undesired segregation of the metal phase in zeolites during calcination; amorphous Fe_2O_3 with a well-structured and enlarged surface was developed under oxygen or argon glow discharge. Ogata et al. [17] suggested that NTP could directly activate lattice oxygen and the surface OH group on TiO_2 catalyst in their study of the decomposition of $CClF_3$.

Proton exchanges and acid–base reactions could occur at the interface between a plasma phase and an aqueous or solid target [18]. Enhancement in acidity by NTP treatment has been reported by Yu et al. [19], in that the Brønsted acidity of the Fe-Mo/HZSM-5 zeolite catalyst was greatly increased. NTP glow discharge treatment approximately doubled both Brønsted and Lewis acid sites on HZSM-5 catalysts, and thus improved the interaction between PdO and HZSM-5, and also improved the dispersion of PdO [20].

Among the value-added chemicals that can be derived from glycerol, acrylic acid, which produced via the intermediate glycerol dehydration to acrolein, received much attention, because this appears to be one of the most promising ways to valorize glycerol [21,22]. Extensive efforts have been committed in recent years to improve glycerol dehydration to acrolein, including glycerol conversion in sub- and supercritical water [23], as well as selective gas-phase conversions [24–30]. Although these different processes gave good glycerol conversion and selectivity to acrolein, a continuous process catalyzed by solid acids is desirable for industrial application. Several catalyst factors are critical to the gas-phase dehydration of glycerol to acrolein. (1) Large surface area is preferred, since it usually positively associates with more active sites. (2) Good dispersion of acid on a support surface and homogeneous distribution of the active compounds would contribute to the catalytic selectivity and a decreased sensitivity to poisoning [1]. (3) Brønsted acid sites are preferred over Lewis acid sites for acrolein formation [22]. Improvement in each of these factors by NTP has been observed in previous studies [1] on NTP applications in catalyst preparation. Consequently, the questions become whether these effects can be attained for supported acid catalysts and whether NTP can help the acid catalyst achieve better catalytic performance in glycerol dehydration to acrolein. To the best of our knowledge, there have been no studies conducted on the NTP modification of solid acid catalysts for dehydration reactions. This study would contribute to further interest in the NTP application in catalysis area. Supported silicotungstic acid has been proven as one of the best performers among many studied catalysts in achieving high yield for the glycerol-to-acrolein conversion [22,27,31]. Therefore, the objective of this study was to investigate how NTP can modify the properties of solid acid catalysts of supported silicotungstic acid in terms of the surface area, the acid strength, the acid dispersion, the type of acid sites, and eventually the catalytic activity in glycerol dehydration to acrolein.

2. Results and Discussion

2.1. BET Surface Area

The measured BET surface areas are listed in Table 1, where the trend that NTP discharge enlarged the surface area is observed. For the unloaded supports, both the NTP-argon and NTP-air increased the surface area, when compared to the original untreated supports. The same trend can be observed for the supported catalysts (HSiW-Al and

HSiW-Si). Particularly, the NTP-argon fabricated ones appeared to have a larger surface area than the NTP-air fabricated counterparts.

Table 1. Brunauer–Emmett–Teller (BET) surface area of the supports and the catalysts with and without nonthermal plasma (NTP) treatment.

	Support (m^2/g)			Supported HSiW (m^2/g)		
	Original	NTP-argon	NTP-air	Regular	NTP-argon	NTP-air
Al	148 ± 4 *	155 ± 1	153 ± 4	140 ± 3	150 ± 2	145 ± 5
Si	393 ± 4	405 ± 6	405 ± 1	300 ± 10	325 ± 9	310 ± 7

* Mean and standard error of three measurements.

2.2. XRD Patterns

XRD patterns of Al-supported and Si-supported catalysts are presented in Figure 1A,B, respectively, together with those of the respective blank support and HSiW powder. Evidently, the HSiW was well dispersed on both Al and Si. Usually, a material with a mesoporous structure would show a large peak in the low angle region (0°–2°) of the XRD patterns [32–34]. Although our XRD scan could only start from 2° due to the instrument limitation, there would be a steep decline line around 2°, if there was a large peak in the low angle region. This decline for a NTP fabricated catalyst was steeper than that for the regular counterpart. Further, the decline for a NTP-argon fabricated catalyst was steeper than that for the NTP-air fabricated counterpart. This could indicate that there was a more distinct mesoporous structure occurring after NTP exposure, or that the mesoporous structure of a support was better retained after the loading of HSiW if NTP was applied during the fabrication. This tendency was more obvious for Si-supported catalysts, which can be explained by assuming that the electron bombardment etched the surface of the catalyst, opening up some micropores, and converting them into mesopores. Since the Si has narrower pores, the existence of the NTP field facilitated the diffusion of the HSiW molecules into the pores instead of clustering at the pore entrances. The results implied that, after NTP exposure, the mesoporous structure was preserved to a large degree while reducing the loss of surface area due to the loading of HSiW.
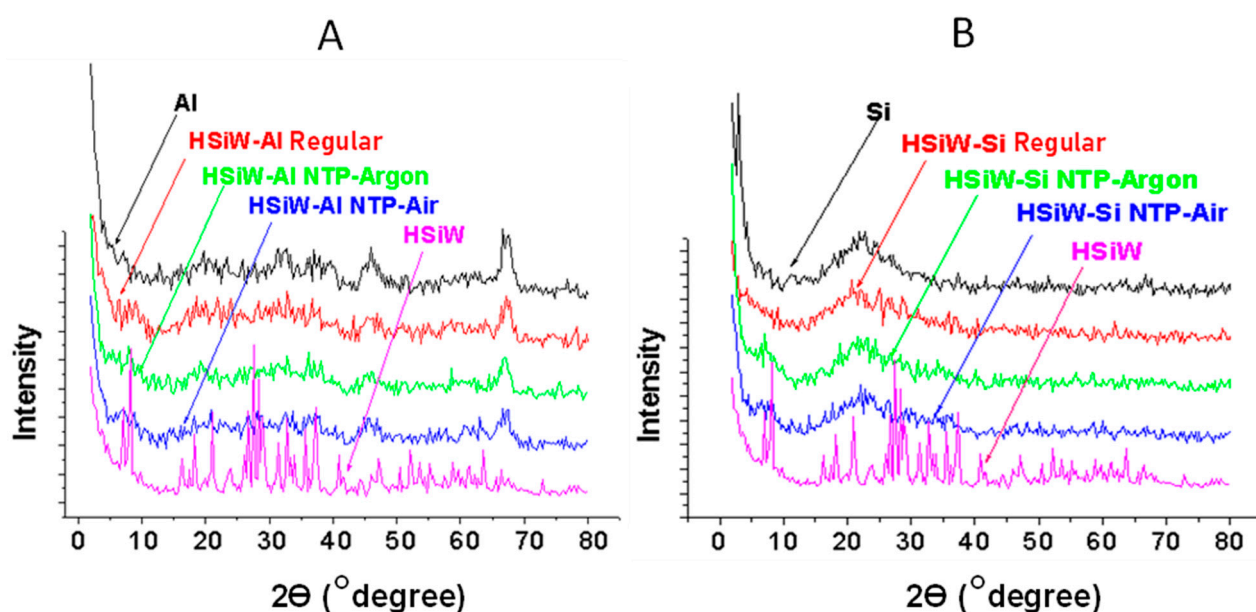
Figure 1. XRD patterns of (**A**) Al-supported and (**B**) Si-supported catalysts together with the respective blank support and HSiW powder.

2.3. TPD-NH₃ for Acid Strength

Figure 2 shows the TPD-NH$_3$ desorption profiles of the catalysts. The peak desorbed at a higher temperature indicates higher acid strength, while a higher TCD signal indicates a larger amount of acid sites. Evidently, the acid strength of the catalysts descended in the order of NTP-argon > Regular > NTP-air for both HSiW-Al (Figure 2A) and HSiW-Si (Figure 2B).
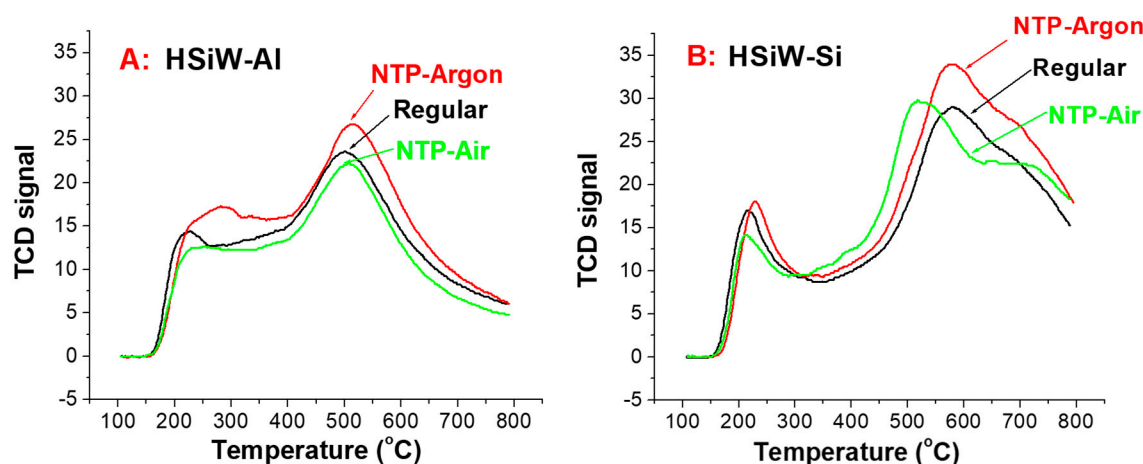

Figure 2. TPD-NH$_3$ desorption profile of (**A**) HSiW-Al and (**B**) HSiW-Si.

2.4. Py-FTIR for Acid Types

TPD-NH$_3$ measures the total acid strength but cannot differentiate the Brønsted acids and Lewis acids. The proportion of these two types of acid sites plays an important role in determining the distribution of products in glycerol dehydration. The Py-FTIR adsorption technique provides a viable measurement of the acid types. Pyridine forms a coordinately bonded complex with a Lewis acid, while it forms pyridinium ion with Brønsted acid sites (as summarized in the table imbedded in Figure 3. In both cases, the N in pyridine shares the lone pair of electrons with acids that have an electron vacancy. Pyridine can also be adsorbed to surface hydroxyl groups via hydrogen bonding. Figure 3 shows the FTIR spectra of pyridine adsorption on HSiW-Al and HSiW-Si fabricated via the regular method without NTP treatment, in comparison to those of the corresponding supports (Al and Si). Two marked peaks (around 1445 cm^{-1} and 1545 cm^{-1}) are commonly acknowledged as the indicators of the Lewis acid sites and the Brønsted acid sites, respectively [35]. For both the blank supports of Al and Si, the signal around 1545 cm^{-1} was hardly differentiated from the baseline noise, indicating that neither of these two supports had significant Brønsted acidity. The hydrogen-bonded pyridine peak (1580–1600 cm^{-1}) [35] was much more distinguished on Si and HSiW-Si, as compared to Al and HSiW-Al. A small peak around 1480 cm^{-1}, which is attributed to both Brønsted acid and Lewis acid, was observed on the Al support, while none was discernable on the Si support. The Al support displayed a relatively larger peak than Si at 1445 cm^{-1}, indicating the higher Lewis acidity of the Al support. Therefore, it can be deduced that both Si and Al had few Brønsted acid sites, and that Al had more Lewis acid sites than Si. Si had more hydrogen-bonded pyridine, which could be attributed to its much larger BET surface area than that of Al; thus, the total number of surface hydroxyl groups was larger on Si than that on Al.
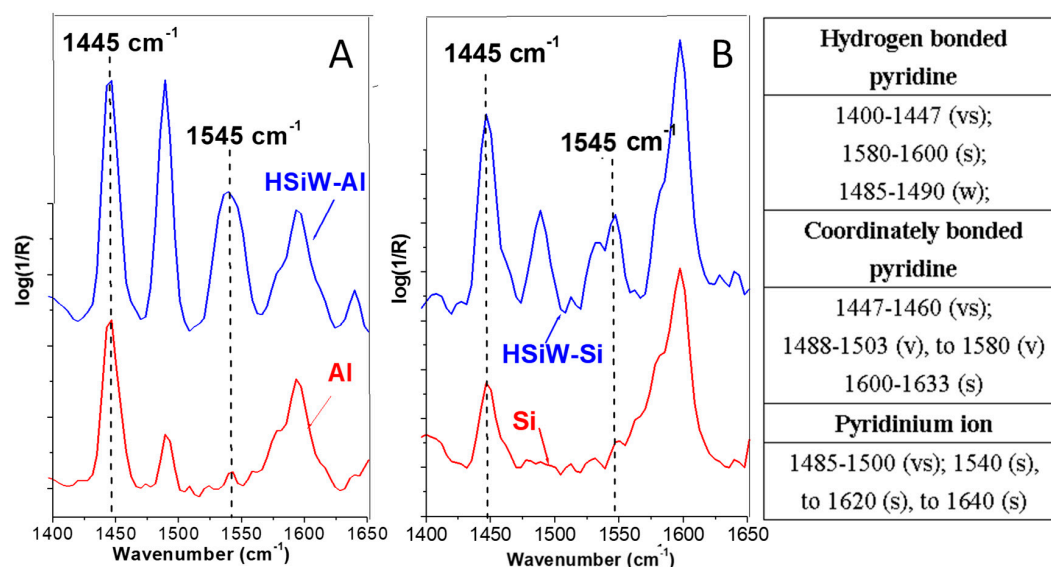
Figure 3. Py-FTIR spectra of (**A**) Al and HSiW-Al (regular 30 wt.% acid loading), and (**B**) Si and HSiW-Si (regular 20 wt.% acid loading). The responsive peak information is summarized in the imbedded table (vs: very strong; s: strong; v: variable; w: weak) [35].

The relative amount of Brønsted acid sites was significantly increased after loading HSiW on Si and Al, as indicated by the peak around 1545 cm^{-1}. Consequently, the 1480 cm^{-1} peak (accumulation of both Brønsted and Lewis acidity) also increased accordingly in the Py-FTIR spectra of HSiW-Al and HSiW-Si.

Figure 4 shows the Py-FTIR spectra of HSiW-Al and HSiW-Si prepared via NTP-argon and NTP-air fabrication, in contrast to those of the regularly fabricated counterparts. The ratio of the signal intensity at 1545 cm^{-1} to that at 1445 cm^{-1} could be used as a measure of the relative amount of Brønsted acid sites to Lewis acid sites on a catalyst surface [36–38]. This ratio was calculated and marked as B/L in Figure 4. For both the HSiW-Al and HSiW-Si, the B/L descended in the order of NTP-argon > NTP-air > Regular, revealing that (1) the NTP treatment either induced higher Brønsted acidity or converted some Lewis acidity to Brønsted acidity, and (2) the NTP-argon fabrication was more effective than NTP-air fabrication in producing more Brønsted acid sites.
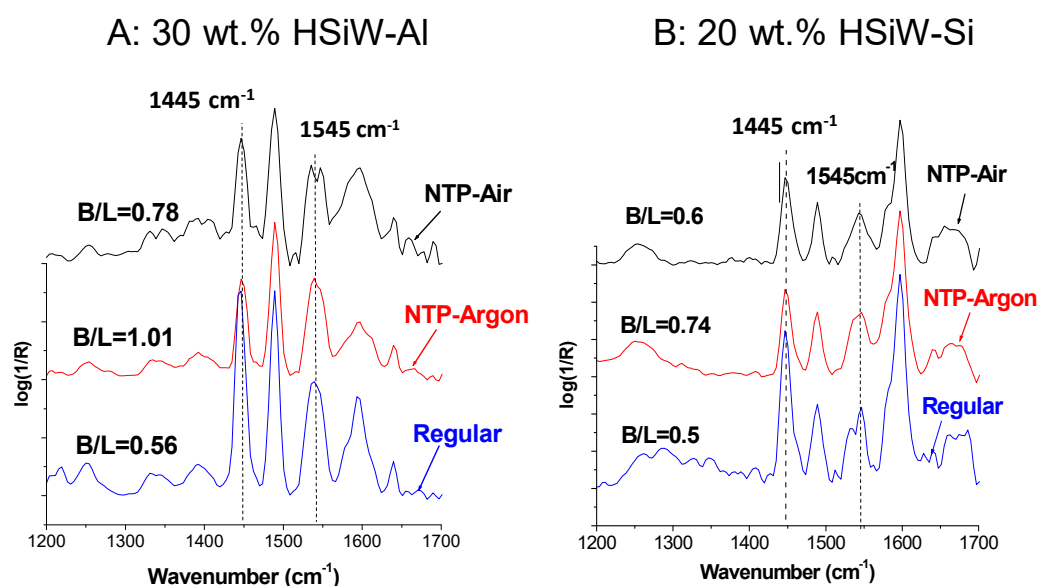
Figure 4. Py-FTIR spectra of NTP treated (**A**) HSiW-Al; (**B**) HSiW-Si in contrast to regularly fabricated counterparts (B/L: ratio of Brønsted acid sites to Lewis acid sites).

2.5. Catalyst Performance in Glycerol Dehydration

The results of the gas-phase glycerol dehydration reactions using the NTP-argon and NTP-air fabricated catalysts are presented in Table 2; the results obtained with their regular counterparts are also provided for comparison. The NTP-argon catalysts showed some improvement in both glycerol conversion and acrolein selectivity; however, the NTP-air catalysts did not show an improvement in term of acrolein selectivity, as compared to the performance of the regular catalyst. In comparison to the Si-supported catalysts, the Al-supported catalysts resulted in higher selectivity towards acetol due to its higher Lewis acidity, in agreement with the literature report [22].

Table 2. Results of glycerol dehydration using HSiW-Al and HSiW-Si catalysts.

		Conversion (mol%)	Selectivity (mol%)				Coke [b] (wt.%)
			Acrolein	Acetaldehyde	Propionaldehyde	Acetol	
HSiW-Al	Regular	96.2 ± 0.3 [a]	77.0 ± 0.9	1.9 ± 0.1	1.4 ± 0.1	10.6 ± 0.9	8.65 ± 0.92
	NTP-Argon	98.9 ± 1.8	80.3 ± 1.1	1.9 ± 0.4	1.5 ± 0.1	10.2 ± 0.7	8.48 ± 0.35
	NTP-Air	96.8 ± 0.9	76.8 ± 1.5	1.7 ± 0.2	1.2 ± 0.1	11.4 ± 1.2	8.06 ± 0.89
HSiW-Si	Regular	92.9 ± 0.6	79.5 ± 0.2	1.1 ± 0.2	1.1 ± 0.0	7.6 ± 0.3	14.27 ± 0.50
	NTP-Argon	93.5 ± 1.8	84.1 ± 0.9	1.2 ± 0.2	1.1 ± 0.1	6.9 ± 0.9	11.67 ± 1.13
	NTP-Air	94.8 ± 1.2	78.7 ± 1.4	1.1 ± 0.3	0.9 ± 0.1	7.5 ± 0.4	11.23 ± 0.56

[a] Mean and standard error of three repetitions over 1.5-7.5 h time-on-stream. [b] Calculated by the catalyst weight gain divided by the fresh catalyst weight after 7.5 h of time-on-stream.

Although the NTP-air treatment did not improve catalyst performance in terms of selectivity toward acrolein, both the NTP-air and NTP-argon treated catalysts resulted in slightly higher glycerol conversion and lower coke formation during the 7.5 h time-on-stream (TOS) compared to the regularly prepared catalyst. The HSiW-Si catalysts obviously had higher coking rate than the HSiW-Al catalysts due to difference in their textures. In our previous study using a regular catalyst, we found no difference in XRD patterns between the fresh catalyst and spent catalyst in that the deposited coke was amorphous and would not change the crystalline structure of the catalyst on which it was deposited. Importantly, the coke formation significantly decreased the glycerol conversion with only minor impact on the selectivity to acrolein; with periodic regeneration using oxygen-containing NTP at low temperatures, the glycerol conversion could be effectively restored [25].

Compared to the regularly prepared catalyst, the result that the NTP-argon fabricated catalysts improved acrolein selectivity agreed well with our TPD-NH$_3$ and Py-FTIR results in that Brønsted acidity and stronger acid strength favored acrolein formation [22]. The preservation of pore size during HSiW loading and the enlargement of the surface area due to the application of NTP were the possible causes of less coke formation, especially for HSiW-Si.

2.6. Possible Mechanisms and Further Research Needs

The interaction between HSiW and the Si support might not be the same as that between HSiW and Al support, because of the difference in the supports' pore structures and especially surface hydroxylation, which might have played an important role in the HSiW adsorption. Since Si has no surface basicity and very weak surface acidity, the coordination mechanism [39] might have predominated the HSiW adsorption on the Si. In this mechanism, an outer-sphere surface complex, $(SiOH_2)^+(SiW)^-$, was formed between the protonated surface hydroxyl and the heteropolyanion, denoted as $(SiW)^-$ (Equation (1)).

With its hydroxylation characteristics, Al has both surface acidity and basicity to certain degree, providing some ionic interaction with HSiW, and thus stronger immobilization of HSiW on its surface, as compared to that on Si surface. The two-step ligand exchange mechanism [39] might occur on the Al surface, where the protons of strong

Brønsted-acidic HSiW first transferred to the Al surface hydroxyl group (Equation (2)), and then the protonated surface hydroxyl group reacted with the heteropolyanion, forming a monolayer neutral surface compound Al(SiW) (Equation (3)). The coordination mechanism could also exist in the interaction between HSiW and Al surface [40], and $(AlOH_2)^+(SiW)^-$ was formed as shown in Equation (1).
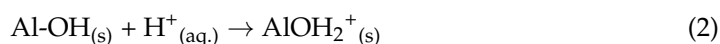
Coordination mechanism:

$$M\text{-}OH_2^+{}_{(s)} + (SiW)^-{}_{(aq.)} \rightarrow (MOH_2)^+(SiW)^- \tag{1}$$
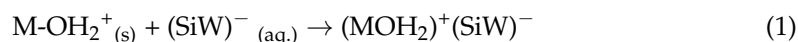
where M is either Al or Si.

Ligand exchange mechanism:

$$Al\text{-}OH_{(s)} + H^+{}_{(aq.)} \rightarrow AlOH_2^+{}_{(s)} \tag{2}$$

$$Al\text{-}OH_2^+{}_{(s)} + (SiW)^-{}_{(aq.)} \rightarrow Al(SiW)_{(s)} + H_2O_{(l)} \tag{3}$$

NTP fabricated catalysts tended to have larger surface area and better preserved mesoporous structures while reducing the loss of the surface area due to the acid loading (Table 1 and Figure 1). Such results could be understood as follows. (1) Continuous electron (or maybe Ar^+) bombardment caused defect sites in the long chain of Si-O-Si or Al-O-Al, and some defect sites (either electron-rich or electron-deficient) might link with neighboring defect sites, resulting in "migration". Such "migration" would possibly cause the conversion of micropores into mesopores. (2) The application of NTP might have increased the interaction between the HSiW molecules and the support (Al or Si), and consequently shortened the distance between HSiW and the support surface. As a result, the pores did not shrink as much as compared to the regular acid loading. (3) During the vaporization of excessive water in the regular fabrication process, the mass transport of the water molecules from bulk liquid possibly pushed some HSiW molecules outward, resulting in some agglomeration at the entrance of the micropores instead of deeply within the pores. Such an event might have been minimized in the presence of NTP, because an additional electrical field existed along with the NTP discharge and this electrostatic force contributed to keeping the HSiW molecules close to the surface (both the outside surface and the wall inside all the pores).

Some plausible mechanisms regarding the increase in acid strength (Figure 2) and Brønsted acidity (Figure 4) are provided here. Each surface OH group is a potential Brønsted acid site, since it is available to be protonated. NTP exposure caused defects on the support surface; such defects are usually associated with surface OH groups. As a result, these newly formed surface OHs by NTP could potentially introduce extra Brønsted acid sites in the presence of water, producing protons (or hydronium ions). These protons countered some of the basic sites on the Al, resulting in a decreased interaction with HSiW. This decreased interaction possibly led to better preservation of the HSiW Keggin structure and a more protonated surface, stoichiometrically resulting in some free hydroxonium. Evidently, our Py-FTIR results revealed some increase in the ratio of Brønsted-pyridine intensity to Lewis-pyridine intensity. The overall acid strength and selectivity to acrolein were also increased for the NTP-argon catalyst, as indicated by our results of TPD-NH_3 and glycerol dehydration experiment.

Regarding that the NTP-air fabrication did not perform as well as the NTP-argon, the following reasons are provided. (1) Because air is more difficult to discharge than argon, the energy and amount of electrons in the NTP-air fabrication were lower than those in the NTP-argon. Consequently, the electron bombardment and ensuing acidity induction by NTP were reduced. (2) As illustrated in process A in Figure 5, dehydroxylation occurred on the surface hydroxyl during calcination in the regular catalyst fabrication procedure. Some dehydroxylated sites were rehydroxylated (process B in Figure 5) when they were again exposed to water during the subsequent loading step, resulting in some Brønsted acid sites. However, during the NTP-air fabrication, some novel surface bonds (Al-O*) could be formed [41,42] (process C in Figure 5). Al-O* was not able to undergo the dihydroxylation–

rehydroxylation process; instead it converted back to the surface hydroxyl group and released oxygen (process D in Figure 5) in the subsequent acid loading. As the result, Brønsted acid sites could not be generated. The released oxygen could either occupy the surface acid sites, blocking the interaction with HSiW, or push outwards the acid via the "degassing" motion. (3) The O atoms formed in NTP were electrophilic. In some sense, all the electrophiles can be considered as acids. These electrophiles had a tendency to be attracted to catalyst surface due to the electrostatic field. Some surface adsorptive sites could be preoccupied by these O atoms, competing with the adsorption of the HSiW anion. Consequently, the binding between HSiW and the support was weakened. The NTP discharge conditions used this study appeared not able to implant the O as lattice oxygen. During calcination, temperature elevation pushed the oxygen atoms off the catalyst surface and they subsequently recombined to molecular O_2. Therefore, the overall NTP-air fabrication did not result in any improvement, or even a hint of negative effect, for acrolein selectivity.

Figure 5. Scheme of surface reactions when the support (Al as example) is dehydrated, hydrated, or exposed to NTP-air.

Although limited improvement of the catalyst performance was achieved in this study, we would like to share some ideas for using novel NTP technology in catalyst fabrication for further investigation.

1. More electrons with higher energy can be produced under the application of a more intense discharge (e.g., higher electric field strength). It is reasonable to deduce that more significant improvement can be achieved by using a more intense NTP-argon discharge.

2. No significant advantage due to the application of NTP was shown in terms of the acid dispersion, since the acid was already well-dispersed on the catalyst surface. With the enhanced electrostatic attraction in NTP fabrication, the loading limit could possibly be pushed higher, which would enhance the Brønsted acidity.

3. In our fabrication procedure, NTP was not applied until most water was evaporated; therefore, how the interaction between the support and HSiW when they first come into contact could be altered by the NTP has not yet been examined. It would be interesting to examine the NTP application at the onset of the wet impregnation. Isometric impregnation is recommended as the acid-loading protocol in future studies.

4. NTP discharge could strengthen the bonding between the catalyst support and HSiW, which could be used as a replacement for calcination. Microwave NTP would be the preferred candidate for this purpose.

3. Materials and Methods

3.1. NTP Apparatus

A plate-to-plate configuration was utilized in this dielectric barrier discharge (DBD) device. As illustrated in Figure 6, two Pyrex glass plates (102 × 102 × 1.6 mm) were separated by a thin-sliced glass tube (large glass ring, 89 mm OD, 1 mm wall thickness, and 10 mm height), which set the gap for NTP discharge. A round copper tape (64 mm

in diameter) was fixed on the outside surface of each plate in the center to serve as two electrodes. The round shape was used to prevent possible spark generation at a sharp edge of the electrodes (such as right angles if a square electrode was used). The discharge zone was therefore a cylinder with a dimension of 64 mm in diameter and 10 mm in height. Two glass tubes (5 mm ID, 6 mm OD) were fixed on opposite sides of the large glass ring; one was connected to a gas tank (gas inlet), and the other was connected to a 150 Torr vacuum supply (gas outlet). Another thin-sliced glass tube (small glass ring, 64 mm ID, 1 mm wall thickness, and 7 mm height) was placed inside the discharge zone to keep the catalyst particles within the NTP discharge. The discharge zone was sealed. The flow rate of a gas supply at 20 mL/min was controlled via a rotameter. The two types of discharge gas used in this study were argon (industrial grade, 99.99%) and air (breathing grade). The NTP field strength used in this study was 9 kV/cm at 1 kHz of frequency.
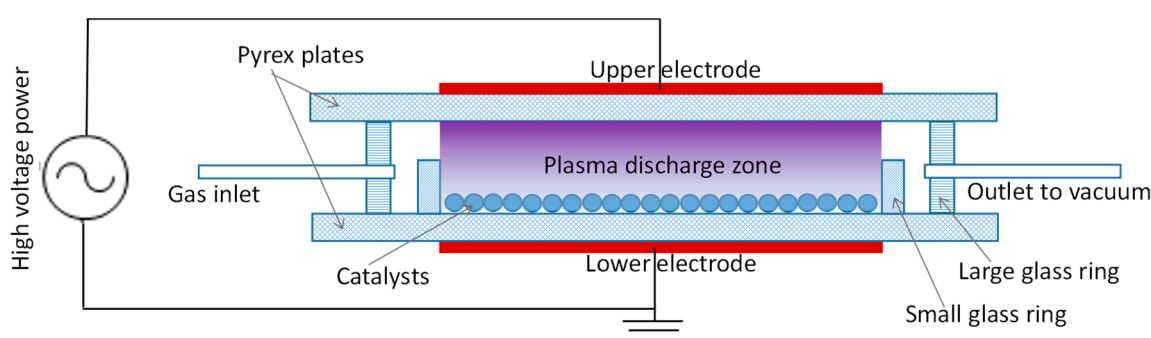
Figure 6. Schematic of NTP fabrication apparatus.

3.2. Procedure of Catalyst Fabrication with NTP

Alumina (Al_2O_3) and silica (SiO_2) are two of the most common supporting materials used in the industry for providing large surface area to accommodate various desired chemical reactions. Mesoporous Al_2O_3 (Davicat®Al2700, 1.2–2.4 mm granules, average pore diameter of 29.9 nm) and SiO_2 (Davicat®Si1252, 1–3 mm granules, average pore diameter of 11 nm) were supplied by Grace-Davison Corp. (Columbia, MD, USA). Both the Al2700 (hereafter abbreviated as Al) and Si1252 (hereafter abbreviated as Si) supports were calcined at 300 °C for 2 h before use. Silicotungstic acid ($H_4SiW_{12}O_{40}\cdot24H_2O$, hereafter abbreviated as HSiW) was purchased from Sigma Aldrich (St. Louis, MO, USA).

The HSiW was loaded on a catalyst support using the wet impregnation method. In this procedure, HSiW was dissolved (10% of the weight of the support) in deionized water to make a 0.04 g/mL solution. A calcined support was added to the HSiW solution. Constant stirring was applied at room temperature for 24 h to attain the adsorption–desorption equilibrium. Afterwards, the catalyst was dried in a convective oven at 55 °C until most water was evaporated and the catalyst was covered only by a thin layer of liquid. The damp catalyst was transported to the NTP apparatus, and arranged in a single layer (no stacking of the particles) to be exposed to the NTP discharge of argon or air for 5 h. Subsequently, the catalyst was sent back to the convective oven to be dried at 105 °C for 2 h before another round loading of HSiW. This procedure was repeated until 30 wt.% or 20 wt.% of HSiW was loaded onto the Al or Si support, respectively, based on the optimal loading from previous studies [27,43]. Hereafter, "NTP-argon" and "NTP-air" denote the process and fabricated catalyst using argon or air as the discharge gas, respectively. All the fabricated catalysts were calcined at 300 °C before use. A control HSiW catalyst supported on Al or Si was also made via the conventional wet impregnation method in the same way described above but without the NTP treatment step, which is denoted as "Regular". In this way, difference in the performance of the catalysts can be attributed to the NTP treatment.

3.3. Catalyst Characterization

Single-point Brunauer–Emmett–Teller (BET) surface area measurement of the catalysts was conducted on a Pulsar ChemBET TPR/TPD system purchased from Quantachrome Instrument (Boynton Beach, FL, USA). A catalyst (0.10 g) was first degassed at 300 °C in a nitrogen atmosphere. The physisorption was initiated when the sample cell was immersed into a liquid nitrogen bath, and then desorption occurred at room temperature. Both the processes were detected by a thermal conductivity detector (TCD) and recorded on a computer. The detailed protocol is provided in the manual of Pulsar ChemBET TPR/TPD [44]. Nitrogen amount was calibrated by injecting a known volume of pure nitrogen gas (ultra purity) until the peak area of the injected volume was equivalent to that of the desorption peak. In this way, the adsorbed nitrogen volume was known based on the monolayer nitrogen adsorption. The surface area of a catalyst under investigation could be obtained and expressed with a unit of square meters per gram (m^2/g), as shown in Equation (4) [45].

$$SA = \frac{SA_{total}}{w} = \frac{P \cdot V \cdot N \cdot A_{cs} \cdot (1 - P/P_o)}{R \cdot T \cdot w} \tag{4}$$

where SA is the specific surface area, P and P_o are the equilibrium pressure and the saturation pressure of the adsorbate at the temperature of adsorption, respectively, V is the total volume of the adsorbed (or desorbed) nitrogen, N is Avogadro's number, A_{cs} is the cross-sectional area of N_2 molecule (0.162 nm^2), R is gas constant, T is the temperature at which desorption takes place, and w is the weight of the loaded catalyst [44].

The acid strength of a solid catalyst was evaluated via temperature programmed desorption of ammonia (TPD-NH_3). The principle of this method is explained as follows. Gaseous base molecules are adsorbed on a catalyst surface, and those adsorbed on stronger acid sites will be more difficult to desorb and will only do so when a higher temperature is applied. As the temperature elevates, the amount of preferentially desorbed base molecules will provide a measure of acid strength of the solid catalyst. Ammonia (NH_3) is the gaseous base that was used, and the TPD-NH_3 measurements were conducted on the Pulsar ChemBET TPR/TPD system. A sample was first pretreated at 100 °C for 1 h in a flow of ultrapure helium gas at 70 mL min^{-1}. This temperature was high enough to fully remove the physisorption of gases (mainly air), while it was also low enough not to affect the subsequent chemisorption. After the pretreatment, the sample was saturated with anhydrous ammonia gas (70 mL min^{-1}) at 100 °C for 30 min, and subsequently flushed with helium (70 mL min^{-1}) at 100 °C for 2 h to remove the physisorbed ammonia. Then heating was applied to ramp the temperature up to 800 °C at a rate of 10 °C min^{-1}. A profile figure was thus obtained with temperature as the x-axis and the TCD signal as the y-axis, which is proportional to the amount of desorbed NH_3. Similar methods have been used to characterize the strength of supported silicotungstic acid for the dehydration of glycerol, showing that different support materials increased thermal stability of the catalysts [46,47].

Powder X-ray diffraction (XRD) patterns of the catalysts were recorded on a Philips X'Pert PRO PW3050 X-ray diffractometer (Malvern Panalytical Inc., Westborough, MA, USA) using Cu *Kα* radiation (0.154 nm) and a graphite generator. The tube voltage and the current were 45 kV and 40 mA, respectively. The scan rate was 0.5° min^{-1}, and the scan range was 2°–80° with a step size of 0.04°.

For the analysis of acid types on the catalysts, Diffuse Reflectance Infrared Fourier Transform Spectroscopy of pyridine adsorption (Py-FTIR) was conducted using a FTIR spectrometer (Excalibur 3100, Varian Inc., Palo Alto, CA, USA) equipped with a research grade diffuse reflection accessory (DiffusIR™, PIKE Technologies, Madison, WI, USA). Before pyridine adsorption, a self-supported sample without KBr dilution was filled in a sample cell and pretreated at 300 °C under vacuum and flow of helium for 2 h. The sample was cooled down to room temperature and then pyridine vapor was admitted to the cell through a vacuum line at room temperature for 2 h. After evacuating the weakly bound

pyridine at 150 °C for 2 h, the sample was cooled down to room temperature and the FTIR spectra were recorded with 128 scans and a resolution of 4 cm^{-1}.

3.4. Glycerol Dehydration to Acrolein

The supported HSiW catalysts on Al (denoted as HSiW-Al) and Si (denoted as HSiW-Si) fabricated with different methods were tested and compared in glycerol dehydration reactions carried out in a down-flow packed-bed reactor at 275 °C and atmospheric pressure. Detailed description of the experiment and evaluation of catalyst performance can be found in our previous publication [25]. Briefly, the reactor was made of a quartz tube (length 300 mm, ID 19.35 mm, OD 25.3 mm), which was heated by a heating tape evenly wrapped around the outer wall of the quartz tube. The heating tape was controlled by a PID temperature controller to maintain the desired temperature of the catalyst bed. The reactor had an external layer of thermal insulation to minimize the heat loss to the surroundings. Seven milliliters of a catalyst (~3.2 g for HSiW-Si and ~3.6 g for HSiW-Al) were packed at the lower end of the reactor, leaving a sufficient path length for the carrier gas and the glycerol feed to be preheated to the desired temperature before reaching the catalyst bed. The glycerol solution (20 wt.% of glycerol in water) was fed by a syringe pump at 6 mL/hour feeding rate, resulting in an 84 h^{-1} gas hourly space velocity (GHSV) of glycerol. The flow rate of carrier gas argon (Ar) was regulated at 60 mL/min. After 1.5 h of stabilization of reaction, reaction effluent from 1.5–7.5 h of time-on-stream was condensed, collected, and analyzed using a gas chromatography equipped with a flame ionization detector (GC-FID) and a VB-WAX capillary column (Valco Instrument Co. Inc., Houston, TX, USA).

The major reaction catalyzed by the solid acid catalysts is the glycerol dehydration to acrolein as shown in Equation (5). Therefore, glycerol conversion (Equation (6)) and acrolein selectivity (Equation (7)) were used to evaluate the catalyst performance.

$$H_2C(OH)CH(OH)CH_2(OH) \rightarrow CH_2=CH-CHO + 2H_2O \tag{5}$$
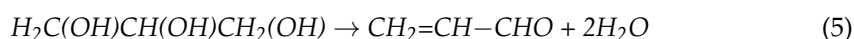
$$X_{glycerol} = \frac{n_{reacted}}{n_{feed}} \times 100\% = \frac{n_{feed} - n_{quantified}}{n_{feed}} \times 100\% \tag{6}$$

where $X_{glycerol}$ is glycerol conversion (mol%), $n_{reacted}$ is the moles of glycerol reacted, n_{feed} is the moles of glycerol in the feed, and $n_{quantified}$ is the remaining glycerol in the collected sample quantified by GC-FID.

$$S_{acrolein} = \frac{n_{c-acrolein}}{n_{c-gly-reacted}} \times 100\% \tag{7}$$

where $S_{acrolein}$ is the selectivity to acrolein (mol%), $n_{c-acrolein}$ is the moles of carbon in the produced acrolein, and $n_{c-gly-reacted}$ is the moles of carbon in the converted glycerol.

Undesirable side reactions also led to the formation of acetol, acetaldehyde, and propionaldehyde [22], which were quantified in the same way using GC-FID. The formation of coke is the most undesirable, as it would deactivate the catalysts [25]. Coke is a distribution of complex carbonaceous species, and it is almost impossible to know the exact chemical content of coke. In this study, the coke formation was calculated as percentage weight gain by catalyst weight gain at the end of 7.5 h of time-on-stream divided by the fresh catalyst weight.

4. Conclusions

The application of NTP to catalyst fabrication demonstrated the potential of modifying the supported silicotungstic acid (HSiW) on Al and Si. The beneficial effects included increasing the surface area, preserving the mesoporous structure, increasing the acid strength, and increasing the proportion of Brønsted acid sites. NTP-argon fabrication provided more significant improvement to the supported HSiW than did the NTP-air fabrication, and the improvement was manifested in glycerol dehydration to acrolein.

However, the NTP-air fabrication did not render significant improvement, indicating that the discharge gas and related plasma chemistry should be important considerations in further studies toward better catalysts.

References

1.　Liu, C.J.; Vissokov, G.P.; Jang, B.W.L. Catalyst preparation using plasma technologies. *Catal. Today* **2002**, *72*, 173–184. [CrossRef]
2.　Kizling, M.B.; Jaras, S.G. A review of the use of plasma techniques in catalyst preparation and catalytic reactions. *Appl. Catal. A Gen.* **1996**, *147*, 1–21. [CrossRef]
3.　Palma, V.; Cortese, M.; Renda, S.; Ruocco, C.; Martino, M.; Meloni, E. A Review about the Recent Advances in Selected NonThermal Plasma Assisted Solid-Gas Phase Chemical Processes. *Nanomaterials* **2020**, *10*, 1596. [CrossRef]
4.　Halverson, D.E.; Cocke, D.L. Ruthenium impregnation of plasma grown alumina films. *J. Vac. Sci. Technol. A* **1989**, *7*, 40–49. [CrossRef]
5.　Khan, H.R.; Frey, H. RF plasma spray deposition of LaMOx (M-equivalent-to-Co, Mn, Ni) films and the investigations of structure, morphology and the catalytic-oxidation of CO and C_3H_8. *J. Alloy. Compd.* **1993**, *190*, 209–217. [CrossRef]
6.　Vissokov, G.P. On the plasma-chemical synthesis and/or regeneration of ultradispersed catalysts for ammonia production. *Catal. Today* **2002**, *72*, 197–203. [CrossRef]
7.　Sugiyama, K.; Anan, G.; Shimada, T.; Ohkoshi, T.; Ushikubo, T. Catalytic ability of plasma heat-treated metal oxides on vapor-phase Beckmann rearrangement. *Surf. Coat. Technol.* **1999**, *112*, 76–79. [CrossRef]
8.　Sugiyama, K.; Nakano, Y.; Aoki, H.; Takeuchi, Y.; Matsuda, T. High-speed preparation of metal oxide fine powders by microwave cold plasma heating. *J. Mater. Chem.* **1994**, *4*, 1497–1501. [CrossRef]
9.　Zhang, Y.; Chu, W.; Cao, W.; Luo, C.; Wen, X.; Zhou, K. A plasma-activated Ni/α-Al_2O_3 catalyst for the conversion of CH_4 to syngas. *Plasma Chem. Plasma Process.* **2000**, *20*, 137–144. [CrossRef]
10.　Maesen, T.L.M.; Bruinsma, D.S.L.; Kouwenhoven, H.W.; Van Bekkum, H. Use of radiofrequency plasma for low-temperature calcination of zeolites. *J. Chem. Soc. Chem. Commun.* **1987**, *17*, 1284–1285. [CrossRef]
11.　Yagodovskaya, T.V.; Lunin, V.V. Surface modification of cements and zeolite catalysts by glow discharge. *Zhurnal Fizicheskoi Khimii* **1997**, *71*, 775–786.
12.　Davis, R.J.; Boudart, M. Structure of Supported PdAu Clusters Determined by X-ray Absorption Spectroscopy. *J. Phys. Chem.* **1994**, *98*, 5471–5477. [CrossRef]
13.　Diamy, A.-M.; Randriamanantenasoa, Z.; Legrand, J.-C.; Polisset-Thfoin, M.; Fraissard, J. Use of a dihydrogen plasma afterglow for the reduction of zeolite-supported gold-based metallic catalysts. *Chem. Phys. Lett.* **1997**, *269*, 327–332. [CrossRef]
14.　Guo, Y.F.; Ye, D.Q.; Chen, K.F.; He, J.C.; Chen, W.L. Toluene decomposition using a wire-plate dielectric barrier discharge reactor with manganese oxide catalyst in situ. *J. Mol. Catal. A Chem.* **2006**, *245*, 93–100. [CrossRef]
15.　Morent, R.; De Geyter, N.; Verschuren, J.; De Clerck, K.; Kiekens, P.; Leys, C. Non-thermal plasma treatment of textiles. *Surf. Coat. Technol.* **2008**, *202*, 3427–3449. [CrossRef]
16.　Veprek, S. Preparation of inorganic materials, surface treatment, etching in low pressure plasmas: Present status and future trends. *Plasma Chem. Plasma Process.* **1989**, *9* (Suppl. 1), 29S–54S. [CrossRef]
17.　Ogata, A.; Kim, H.-H.; Futamura, S. Direct activation of catalyst-surface by nonthermal plasma. *Catal. Catal.* **2005**, *47*, 491–493.
18.　Amouroux, J. Interaction between a condensed target and a non-equilibrium plasma: Acid-base reactions at the interface. *Scanning Electron Microsc.* **1987**, *1*, 1575–1592.
19.　Yu, K.-L.; Xia, Q.; Liu, C.-J.; Li, G.; Eliasson, B.; Xue, B. On the plasma enhanced Bronsted acidity of solid acids. In Proceedings of 4th International Symposium On Green Chemistry In China (Part 1), Jinan, China, 14 July 2001.
20.　Liu, C.J.; Yu, K.L.; Zhang, Y.P.; Zhu, X.L.; He, F.; Eliasson, B. Characterization of plasma treated Pd/HZSM-5 catalyst for methane combustion. *Appl. Catal. B Environ.* **2004**, *47*, 95–100. [CrossRef]
21.　Katryniok, B.; Paul, S.; Dumeignil, F. Recent Developments in the Field of Catalytic Dehydration of Glycerol to Acrolein. *ACS Catal.* **2013**, *3*, 1819–1834. [CrossRef]

22. Liu, L.; Ye, X.P.; Bozell, J.J. A Comparative Review of Petroleum-Based and Bio-Based Acrolein Production. *ChemSusChem* **2012**, *5*, 1162–1180. [CrossRef]
23. Cheng, L.; Liu, L.; Ye, X.P. Acrolein Production from Crude Glycerol in Sub- and Super-Critical Water. *J. Am. Oil Chem. Soc.* **2013**, *90*, 601–610. [CrossRef]
24. Cheng, L.; Ye, X.P. A DRIFTS Study of Catalyzed Dehydration of Alcohols by Alumina-supported Heteropoly Acid. *Catal. Lett.* **2009**, *130*, 100–107. [CrossRef]
25. Liu, L.; Ye, X.P.; Katryniok, B.; Capron, M.; Paul, S.; Dumeignil, F. Extending Catalyst Life in Glycerol-to-Acrolein Conversion Using Non-thermal Plasma. *Front. Chem.* **2019**, *7*, 108. [CrossRef] [PubMed]
26. Katryniok, B.; Paul, S.; Belliere-Baca, V.; Rey, P.; Dumeignil, F.; Abdullah, A.Z. Glycerol dehydration to acrolein in the context of new uses of glycerol. *Green Chem.* **2010**, *12*, 2079–2098. [CrossRef]
27. Tsukuda, E.; Sato, S.; Takahashi, R.; Sodesawa, T. Production of acrolein from glycerol over silica-supported heteropoly acids. *Catal. Commun.* **2007**, *8*, 1349–1353. [CrossRef]
28. Chai, S.-H.; Wang, H.-P.; Liang, Y.; Xu, B.-Q. Sustainable production of acrolein: Gas-phase dehydration of glycerol over 12-tungstophosphoric acid supported on ZrO_2 and SiO_2. *Green Chem.* **2008**, *10*, 1087–1093. [CrossRef]
29. Katryniok, B.; Paul, S.; Capron, M.; Lancelot, C.; Bellière-Baca, V.; Rey, P.; Dumeignil, F. A long-life catalyst for glycerol dehydration to acrolein. *Green Chem.* **2010**, *12*, 1922–1925. [CrossRef]
30. Lauriol-Garbay, P.; Millet, J.M.M.; Loridant, S.; Bellière-Baca, V.; Rey, P. New efficient and long-life catalyst for gas-phase glycerol dehydration to acrolein. *J. Catal.* **2011**, *280*, 68–76. [CrossRef]
31. Atia, H.; Armbruster, U.; Martin, A. Dehydration of glycerol in gas phase using heteropolyacid catalysts as active compounds. *J. Catal.* **2008**, *258*, 71–82. [CrossRef]
32. Varisli, D.; Dogu, T.; Dogu, G. Novel mesoporous nanocomposite WOx-silicate acidic catalysts: Ethylene and diethylether from ethanol. *Ind. Eng. Chem. Res.* **2009**, *48*, 9394–9401. [CrossRef]
33. Baca, M.; Rochefoucauld, E.d.l.; Ambroise, E.; Krafft, J.-M.; Hajjar, R.; Man, P.P.; Carrier, X.; Blanchard, J. Characterization of mesoporous alumina prepared by surface alumination of SBA-15. *Microporous Mesoporous Mater.* **2007**, *110*, 232–241. [CrossRef]
34. Yan, X.-M.; Lei, J.H.; Liu, D.; Wu, Y.C.; Liu, W. Synthesis and catalytic properties of mesoporous phosphotungstic acid/SiO_2 in a self-generated acidic environment by evaporation-induced self-assembly. *Mater. Res. Bull.* **2007**, *42*, 1905–1913. [CrossRef]
35. Tanable, K.; Misono, M.; Ono, M.; Hattori, H. *New Solid Acids and Bases: Their Catalytic Properties, Studies in Surface Science and Catalysis*; Delmon, B., Yates, J.T., Eds.; Elsevier: Tokyo, Japan, 1989.
36. Chakraborty, B.; Viswanathan, B. Surface acidity of MCM-41 by in situ IR studies of pyridine adsorption. *Catal. Today* **1999**, *49*, 253–260. [CrossRef]
37. Sakthivel, R.; Prescotta, H.; Kemnitz, E. WO_3/ZrO_2: A potential catalyst for the acetylation of anisole. *J. Mol. Catal. A Chem.* **2004**, *223*, 137–142. [CrossRef]
38. Musthofa, M.; Karim, A.H.; Fadzlillaah, N.A.; Annuar, N.H.R.; Jalil, A.A.; Triwahyono, S. Determination of Lewis and Brönsted acid sites by gas flow-injection technique. *J. Fundam. Sci.* **2010**, *6*, 127–131. [CrossRef]
39. Wu, Y.; Ye, X.K.; Yang, X.G.; Wang, X.P.; Chu, W.L.; Hu, Y.C. Heterogenization of heteropolyacids: A general discussion on the preparation of supported acid catalysts. *Ind. Eng. Chem. Res.* **1996**, *35*, 2546–2560. [CrossRef]
40. Wang, X.; Ye, X.; Wu, Y. Interaction between 12-Silicotungstic acid (SiW_(12)) and γ-Al2O3 surface. *Chin. J. Catal.* **1996**, *17*, 149–152.
41. Gieshoff, J.; Lang, J. Process for The Plasma-Catalytic Production of Ammonia. U.S. Patent 6471932B1, 29 October 2002.
42. Kameoka, S.; Kuroda, M.; Aoyagi, K.; Ito, S.; Kunimori, K. Formation of novel Al2O3 surface (Al-O-star) by plasma-excited nitrogen and its catalytic application—Production of ammonia and oxygen from nitrogen and water. *Appl. Surf. Sci.* **1997**, *121*, 351–354. [CrossRef]
43. Atia, H.; Armbruster, U.; Martin, A. Dehydration of glycerol in gas phase using heteropolyacid catalysts as active compounds. In Proceedings of the DGMK-Conference "Future Feedstocks for Fuels and Chemicals", Berlin, Germany, 29 September–1 October 2008; pp. 177–184.
44. Quantachrome. *User Manual for ChemBET Pulsar TPR/TPD*; Quantachrome Instrument: Boynton Beach, FL, USA, 2008; pp. 94–96.
45. Lowell, S.; Shields, J.E.; Thomas, M.A.; Thommes, M. *Characterization of Porous Solids and Powders: Surface Area, Pore Size and Density*; Particle Technology Series; Scarlett, B., Ed.; Springer: Dordrecht, The Netherland, 2004.
46. Talebian-Kiakalaieh, A.; Saidina Amin, N.A. Gas phase glycerol dehydration to acrolein using supported silicotungstic acid catalyst. *Malays. J. Anal. Sci.* **2017**, *21*, 849–859.
47. Katryniok, B.; Paul, S.; Capron, M.; Bellière-Baca, V.; Rey, P.; Dumeignil, F. Regeneration of Silica-Supported Silicotungstic Acid as a Catalyst for the Dehydration of Glycerol. *ChemSusChem* **2012**, *5*, 1298–1306. [CrossRef] [PubMed]